Available online at www.sciencedirect.com
ScienceDirect
Journal of Nuclear Materials 363–365 (2007) 522–527
journal of nuclear materials
www.elsevier.com/locate/jnucmat

Edge harmonic oscillations at the density pedestal in the H-mode discharges in CHS Heliotron measured using beam emission spectroscopy and magnetic probe

S. Kado [a,*], T. Oishi [b], M. Yoshinuma [c], K. Ida [c], M. Takeuchi [d], K. Toi [c], T. Akiyama [c], T. Minami [c], K. Nagaoka [c], A. Shimizu [c], S. Okamura [c], S. Tanaka [b], CHS Group [c]

[a] *High Temperature Plasma Center, The University of Tokyo, Kashiwanoha, Kashiwa, Chiba 277-8568, Japan*
[b] *School of Engineering, The University of Tokyo, Bunkyo-ku, Tokyo 113-8656, Japan*
[c] *National Institute for Fusion Science, Toki, Gifu 509-5292, Japan*
[d] *Department of Energy Engineering and Science, Nagoya University, Nagoya 464-8603, Japan*

Abstract

Edge harmonic oscillations (EHO) offer the potential to relax the H-mode pedestal in a tokamak, thus avoiding edge localised modes (ELM). The mode structure of the EHO in CHS was investigated using a poloidal array of beam emission spectroscopy (BES) and a magnetic probe array. The EHO exhibited a peculiar characteristic in which the first, second and third harmonics show the same wavenumber, suggesting that the propagation velocities are different. Change in the phase of higher harmonics at the time when that of the first harmonic is zero can be described as a variation along the $(m,n) = (-2,1)$ mode structure, though the EHO lies on the $\iota = 1$ surface. This behavior leads to an oscillation that exhibits periodic dependence of shape on spatial position.

PACS: 52.35.−g; 52.35.Py; 52.55.Hc; 52.70.Kz

Keywords: Transport barrier; Spectroscopy; Fluctuations and turbulence

1. Introduction

Edge harmonic oscillation (EHO) has been observed in quiescent high confinement (QH)-mode in several tokamaks, such as DIII-D [1], ASDEX Upgrade [2], JET [3] and JT-60U [4]. EHO has drawn attention because of its potential to provide moderate particle exhaust without ELM activities that may be desirable for the steady-state operation of forthcoming fusion devices.

Recently, EHO-like coherent MHD activities have also been observed in helical devices, such as the large helical device (LHD) [5] and the compact

* Corresponding author. Tel.: +81 3 5841 7667; fax: +81 3 5802 7221.
E-mail address: kado@q.t.u-tokyo.ac.jp (S. Kado).

0022-3115/$ - see front matter © 2007 Elsevier B.V. All rights reserved.
doi:10.1016/j.jnucmat.2006.12.039

helical system (CHS) [6]. The EHO in CHS was first identified using a beam emission spectroscopy (BES) with a radial fiber array; soon thereafter, it was recognized to be clearly observable using a magnetic probe array.

In CHS H-mode discharges with an edge particle transport barrier, a transition phenomenon characterized by a sudden drop in the temporal evolution of the H_α intensity can be observed when the heating power exceeds a certain threshold – note that ELM activities are not apparent in CHS. We categorize the typical waveform into three phases: (1) the L-phase before the transition, (2) the density build-up phase, and (3) the ETB-saturation phase.

EHOs having a fundamental frequency of 4.5 kHz (in the magnetic axis position $R_{ax} = 92.1$ cm, toroidal magnetic field strength at the magnetic axis $B_{ax} = 0.95$ T geometry) and a second harmonic are observed when the density gradient of the pedestal reaches a certain threshold.

There are many similarities between the EHOs in tokamaks and those in a CHS [6]. In particular, the mode exists in the steep pressure/density gradient region where a rational surface is also located. From the radial fiber array for the BES, the EHO of a CHS has been revealed to be localized around the $\iota = 1$ surface.

On the other hand, the mode structure of the EHO seems to depend on the devices, even differing between tokamaks. From the poloidal magnetic probe array, the poloidal mode number was found to be 2.

Since the theoretical explanation of the harmonic frequency is yet to be resolved [7], it is important to clarify the detailed mode structure and/or the poloidal wavenumber for each harmonic in the helical geometry in order to help expose the underlying physics.

In the present study, we changed the observation fiber array from a radial to a poloidal arrangement to analyze the poloidal correlation for the EHO. The results are compared with those obtained using the poloidal and toroidal magnetic probe sets.

2. Experimental setup

CHS is a middle-size low aspect-ratio ($R = 1$ m, $a = 0.2$ m) helical device with the pole number $L = 2$ and the pitch number $M = 8$. An H-mode characterized by a sudden drop of the H_α signal can be achieved by two systems of high-power neutral beam injection (NBI), both of which are installed tangentially to the toroidal field in the ι-increasing direction (called co-injection). After the H-mode transition, the density gradient around the rotational transform $\iota = 1$ surface ($r/a \sim 0.95$) becomes steeper, forming a density pedestal [8,9]. EHO can be observed when the increase in the edge density gradient becomes saturated. The interval between the transition and the onset of EHO depends on the power and magnetic configuration.

For the local measurement of both the density gradient and fluctuations, we have developed a BES system in CHS [10,11]. Emission from the beam atom is governed by collisional processes to populate the excited state. Therefore, the intensity and its fluctuation of the Doppler-shifted beam emission correspond to the density and its fluctuation, respectively [12]. In order to optimize the spatial resolution, viewing optics were located on a port inserted deep inside the vacuum chamber so that the sightlines became tangent to the local magnetic field. One can select 8 channels to be recorded out of 16 viewing chords. A low-pass filter in the avalanche photo detector (APD) circuit limits the obtainable frequency to 100 kHz.

The poloidal BES configuration we applied in the present experiment measures only at a fixed radial position. Therefore, we scanned the position of the magnetic axis so that the position of the EHO matched the observation area – it should be noted that the higher harmonics appear only one or two radial chords while the first harmonic usually exists over wider region [13]. It was revealed to be the $R_{ax} = 91.1$ cm configuration, shown in Fig. 1(a). The corresponding radial position of the sightline is about $r/a \sim 0.9$. The $\iota = 1$ surface located at $r/a \sim 0.97$ is included in this sightline, because the sightline apart from the midplane crosses a wider normalized minor radius than that on the midplane as in the radial configuration. The spatial pitch Δx is 1.3 cm, which yields the Nyquist wavenumber, $k_N = \pi/\Delta x$, of 2.42 rad cm^{-1}.

The poloidal magnetic probe array is schematically shown in Fig. 1(b) [14]. The toroidal magnetic probes are located at every $\pi/4$ radian toroidal angle at $R = 120$ cm on the midplane. We introduced an absolute coordinate system to describe the 3-D mode structure of the EHO. Each probe is labeled by the toroidal (ϕ) and poloidal (θ) angles. The coordinate $\phi = 0$ represents the cross-section at the horizontally elongated poloidal plane while $\theta = 0$ represents the outermost minor radius. In

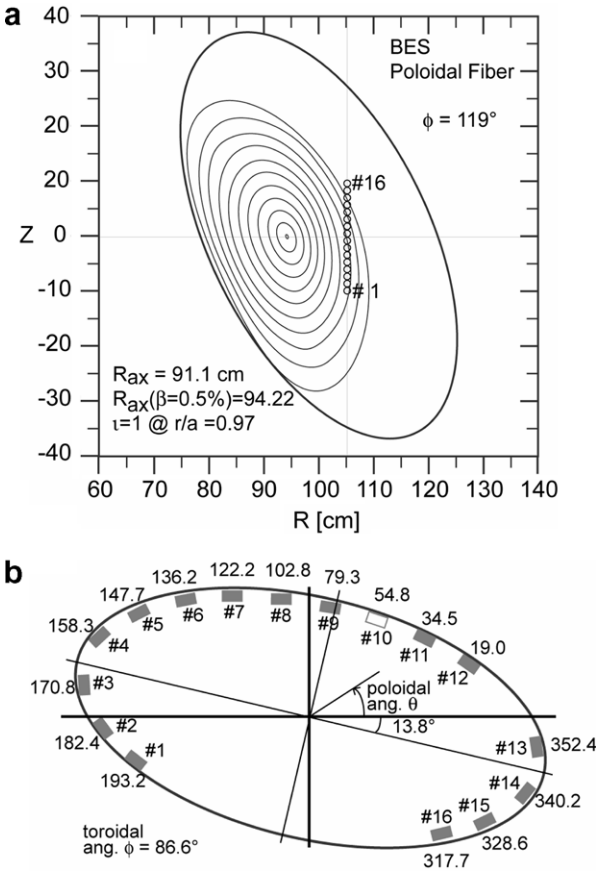

Fig. 1. Observation area of (a) the poloidal BES and (b) the poloidal magnetic probe array.

the present study, signals from the poloidal magnetic probe number #3, 5, 7, 9, and 11 are recorded. Assuming that the EHO occurs on the $\iota = 1$ surface, the spatial pitch of the poloidal array Δx in the present condition is 11 cm, which yields $k_N = 0.29\ \mathrm{rad\ cm^{-1}}$, while that of the toroidal array is $0.031\ \mathrm{rad\ cm^{-1}}$ for $\Delta x = 78$ cm.

Plasma was initiated by ECH during 30–50 ms and further heated by two systems of NBI for 40–140 ms having an injection port-through power of 1.5 MW. The average density before the ETB transition was about $2 \times 10^{13}\ \mathrm{cm^{-3}}$. The waveforms of the diagnostics are similar to those reported in Ref. [6], but there are some differences. In this condition, the EHO can be observed right after the ETB transition: from 80 ms until 115 ms in this case. The fundamental frequency was 3.1 kHz, which is slightly lower than the typical frequency at $R_{\mathrm{ax}} = 92.1$ cm configuration. It should be mentioned that the frequency of the mode varies slightly in time during the discharge.

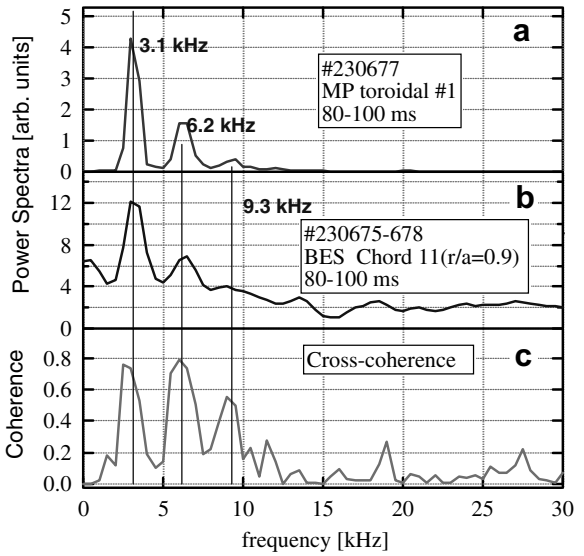

Fig. 2. Frequency spectra from (a) the magnetic probe and (b) the BES. (c) Cross-coherence between the magnetic probe and BES. The third harmonic of EHO can be clearly observed.

As can be seen in Fig. 2, a third harmonic was observed in both BES and magnetic probe signals for the first time in CHS. For BES, 10 ms (between 90 and 100 ms of discharge) times 4 shots were averaged in order to improve the signal-to-noise (S/N) ratio. One can see the clear correlation of the first, second and third harmonics from the cross-coherence.

3. Results

3.1. Spatiotemporal analysis of the EHO

The initial mode analysis from the magnetic probe data suggest that the both first and second harmonic components have the poloidal mode number $m = -2$ (negative m means electron diamagnetic direction), and that they exist near the $\iota = 1$ rational surface, as reported in Ref. [6]. This is one peculiarity in this mode, since the phase velocity $2\pi f/k$ is different for each harmonic. In other words, this is not a simple picture of the MHD mode on the plasma frame.

Therefore, we performed a Fourier analysis with respect to space and time to deduce wavenumber (k)-frequency (f) power spectra. Toroidal (ϕ) and poloidal (θ) wavenumbers are denoted k_ϕ and k_θ, respectively. The results are shown in Fig. 3(a) and (b). From the figure, $m = -2$ ($k_\theta = 0.1\ \mathrm{rad\ cm^{-1}}$,

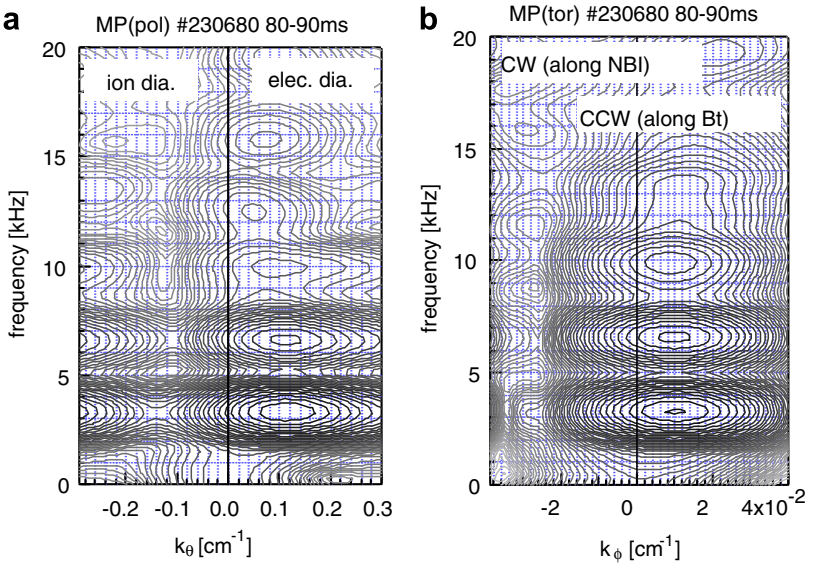

Fig. 3. Power spectra $S(k,f)$ for (a) poloidal and (b) toroidal magnetic probe arrays.

$r = 20$ cm) in the electron diamagnetic direction and $n = 1$ ($k_\phi = 0.01$ rad cm^{-1}, $R = 100$ cm) along the toroidal field direction are determined. As can be seen from the figure, the wavenumber of each harmonic is the same while only the frequency is doubled or tripled; namely, the $(m,n) = (-2,1)$ structure is preserved for higher harmonic frequencies.

3.2. 3-D mode structure of the EHO

We defined the phase of the p-th harmonic oscillation having $(m,n) = (-2,1)$ mode structure as a function of toroidal and poloidal coordinates and time:

$$\begin{aligned}\Phi_p(\phi,\theta,t) &= k_\phi R\phi + k_\theta r\theta - 2\pi pft + \Phi_{0p},\\ &= (\phi - 2\theta) - 2\pi pft + \Phi_{0p}. \end{aligned} \quad (1)$$

Let t_0 be the time at which the phase of the first harmonic is zero at given coordinates;

$$\Phi_1(\phi,\theta,t_0) = (\phi - 2\theta) - 2\pi ft_0 + \Phi_{01} = 0. \quad (2)$$

The phase difference between the p-th ($p \geqslant 2$) and first harmonic at t_0 can be described as

$$\begin{aligned}\Delta\Phi_p &= \Phi_p(\phi,\theta,t_0) - p\Phi_1(\phi,\theta,t_0)\\ &= (1-p)\left(\phi - 2\theta - \frac{\Phi_{0p} - p\Phi_{01}}{1-p}\right). \end{aligned} \quad (3)$$

Therefore, by plotting the phase difference at t_0 as a function of $(\phi - 2\theta)$, one can determine the angle $\phi - 2\theta$, *i.e.*, the 3-D spatial position where the p-th harmonic is in phase with the first harmonic. The least-square fit of the sinusoidal function to the experimental data was performed to the reconstructed Fourier component of each harmonic frequency of the EHO.

The results obtained with poloidal and toroidal magnetic probe arrays are shown in Fig. 4(a). One can see that at $\sigma_0 = \phi - 2\theta = 0.2 \times 2\pi$ rad, every harmonic is in phase with the others. Then, Eq. (3) requires $\Phi_{01} = \Phi_{0p} = \Phi_0$ regardless of p. As the displacement with respect to poloidal or toroidal direction increases, the phase between the harmonics shifts at different rates, with a fitted slope almost equal to $p - 1$. This observation also indicates that each harmonic propagates at a different velocity along the $(m,n) = (-2,1)$ mode structure. This is why the shape of the raw signal changes depending on the angle $\phi - 2\theta$, as shown in Fig. 4(b). This figure tells us that the higher harmonic mode arrives at the spatial position earlier. These results indicate that the initial phases of the harmonic oscillations are locked at particular magnetic field line, but the harmonic modes propagate at the different phase velocity. This is consistent with what we have shown in the k–f power spectra. The question as to why the $(m,n) = (-2,1)$ mode is locked on the $\iota = 1$ surface has yet to be understood.

The BES observed the poloidal cross-section at $\phi = 119°$. The poloidal angles for the 11th ($r/a \sim 0.9$) and 12th ($r/a \sim 0.92$) viewing chords where the EHO signal is detected, are around $\theta = 33$–$42°$.

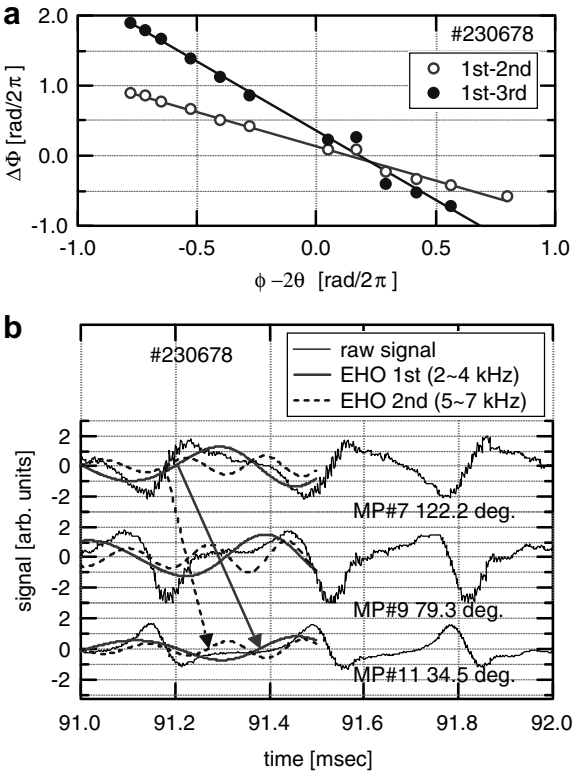

Fig. 4. (a) Phase difference between harmonics. (b) Interpretation of the change in the shape of the raw signals in different spatial positions.

i.e. $\phi - 2\theta = 0.15\text{–}0.10 \times 2\pi$ rad. Due to the poor S/N ratio in the current system, only the first and second harmonic could be observed without the summation of many shots. The average value of the phase difference $\Delta\Phi_2$ (BES) $= 0.05 \times 2\pi$ rad, which is fairly consistent with $\Delta\Phi_2$ (Mag. Probe) $= 0\text{–}0.05 \times 2\pi$ rad.

4. Discussion

As a possible alternative explanation for the constant poloidal mode number of the harmonics described in Section 3.1, we examined the possibility that the magnetic probe arrays detect a beat wavenumber of a higher-m mode. In this case, the real wave number k_{real} might be a multiple of k_N higher than the observed k_{obs} due to the discrete spatial sampling,

$$k_{\text{obs}} = k_{\text{real}} \pm 2Nk_N \quad (N = 1, 2, 3, \ldots), \tag{4}$$

where the negative sign in the right-hand side represents the opposite propagation direction to the real

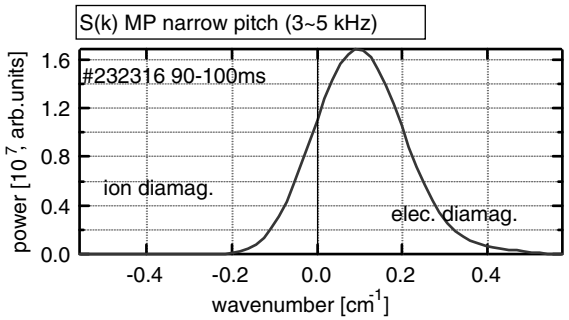

Fig. 5. Wavenumber spectra of poloidal magnetic probe array with narrower pitch.

one. Actually, an alias mode of about $m = 10$ might have appeared in the $m = 2$ range, since the present k-resolution of $k_N = 0.3$ corresponds to $m = 6$.

To test this hypothesis, we conducted an experiment with similar conditions to what we show above, but the pitch of the poloidal magnetic probe array was reduced to half, namely probes #2–#9 in the series depicted in Fig. 1(b), with k_N increased to 0.6 rad cm^{-1} ($m = 12$). The preliminary results in this condition revealed that even though the 2nd harmonic components were not clear, the peak wavenumber for the first harmonic was similar, around 0.1 rad cm^{-1}, as shown in Fig. 5. Therefore, it is unlikely that the magnetic probe picked up the beat frequency of a higher-m mode.

Unfortunately, the wavenumber resolution for BES is about 0.6 rad cm^{-1}, which corresponds to the mode number of 12, while the Nyquist mode number is 48. Therefore, it is difficult to resolve these low-m modes using the present poloidal BES data. Optimization of the fiber chords to observe the single flux surface so as to detect EHOs in all channels is planned in the near future.

5. Summary

The spatial correlation of the EHO in CHS was investigated using the poloidal BES sightlines and the poloidal and toroidal magnetic probe arrays. The following characteristics of the EHO have been recognized:

- The third harmonic was identified at the configuration of $R_{\text{ax}} = 91.1$ cm.
- These harmonics exhibit the same poloidal and toroidal wavenumbers.
- This suggests that they propagate at different phase velocities.

– The phase difference between the harmonics lies on the $(m,n) = (-2,1)$ mode structure.
– This implies that the shape of the row signal depends on the phase parameter $\phi - 2\theta$.

These observations might be an effective test for theoretical models of EHO in the future.

Acknowledgements

This work was supported in part by the NIFS Collaborative Research Program (NIFS02KZPD003).

References

[1] C.M. Greenfield, K.H. Burrell, J.C. DeBoo, et al., Phys. Rev. Lett. 86 (2001) 4544.
[2] W. Suttrop, M. Maraschek, G.D. Conway, et al., Plasma Phys. Control. Fusion 45 (2003) 1399.
[3] W. Suttrop, V. Hynonen, T. Kurki-Suonio, et al., Nucl. Fusion 45 (2005) 721.
[4] N. Oyama, Y. Sakamoto, A. Isayama, et al., Nucl. Fusion 45 (2005) 871.
[5] K. Toi, S. Ohdachi, M. Takechi, et al. Proceedings of the 27th European Physical Society Conference on Controlled Fusion and Plasma Physics, Budapest, vol. 24B, European Physical Society, Geneva, 2000, p. 1328.
[6] T. Oishi, S. Kado, M. Yoshinuma, et al., Nucl. Fusion 46 (2006) 317.
[7] D.R. McCarthy, Phys. Plasmas 9 (2002) 2451.
[8] S. Okamura, T. Minami, C. Suzuki, et al., J. Plasma Fusion Res. 79 (2003) 977. <http://www.jspf.or.jp/Journal/2003.html>.
[9] S. Okamura, T. Minami, T. Oishi, et al., Plasma Phys. Control. Fusion 46 (2004) A113.
[10] T. Oishi, S. Tanaka, S. Kado, M. Yoshinuma, K. Ida, S. Okamura, S. Tanaka CHS group, Rev. Sci. Instrum. 75 (2004) 4118.
[11] T. Oishi, S. Kado, M. Yoshinuma, K. Ida, S. Tanaka, S. Okamura, J. Plasma Fusion Res. Ser. 6 (2004) 449.
[12] R.J. Fonck, P.A. Duperrex, S.F. Paul, Rev. Sci. Instrum. 61 (1990) 3487.
[13] T. Oishi, S. Kado, M. Yoshinuma, et al., Phys. Plasmas 13 (2006) 104504.
[14] S. Sakakibara, H. Yamada, A. Ejiri, et al., Jpn. J. Appl. Phys. 63 (1994) 4406.